Self-assembled complex micelle phase stability in ABA-type triblock copolymers and related core-shell bottlebrushes

Michael G. Karavolias and Mahesh K. Mahanthappa*
Department of Chemical Engineering and Materials Science, University of Minnesota–Twin Cities, 421 Washington Ave. SE, Minneapolis, Minnesota 55455, USA

(Received 30 May 2023; revised 21 October 2023; accepted 6 December 2023; published 31 January 2024)

We report the synthesis and temperature-dependent morphologies of a series of polylactide-*block*-poly(ε-decalactone)-*block*-polylactide (LDL) triblock copolymers with $M_n = 16.0$–18.1 kg/mol and volume fractions $f_L = 0.27$–0.31 and associated core-shell bottlebrush (csBB) polymers, which derive from enchaining LDL triblocks through a polymerizable midchain functionality. While the LDL triblocks form micellar Frank-Kasper A15 and σ phases due to the conformational asymmetry of this monomer pair, the csBB morphologies sensitively depend on the backbone degree of polymerization (N_{bb}). At low N_{bb} values, micellar Frank-Kasper phases with the brush backbone situated in the matrix domain are stable, albeit with a modest reduction in the mean interfacial curvature evidenced by a σ to A15 order-to-order transition. However, larger N_{bb} values drive csBBs to form hexagonally packed cylinders phases. This N_{bb}-dependent phase behavior is rationalized in terms of a star-to-bottlebrush transition. At low N_{bb} values, the csBBs are akin to star polymers with pointlike junctions that can support complex micelle packings. As N_{bb} increases, the csBBs adopt cylindrical molecular geometries with extended backbones situated in the matrix domain that prefer hexagonally packed cylinders morphologies.

DOI: 10.1103/PhysRevMaterials.8.015603

I. INTRODUCTION

The self-assembly of multifunctional block copolymers offers a useful and scalable means for producing designer soft materials [1] with potential applications as advanced separations membranes [2], components in energy conversion devices [3], and nanotemplates for metamaterials [4] and photonic crystals [5]. The self-assembled morphologies of microphase-separated, linear A/B block copolymer melts stem from a delicate interplay of minimizing energetically unfavorable A/B monomer contacts, while minimizing the configurational entropy penalty associated with stretching the polymer chains in an incompressible melt [6–8]. Morphology diagrams for linear AB diblock [9] and ABA triblock [10,11] copolymers based on mean-field theories and corroborated by experiments [12,13] parameterize their phase behaviors in terms of the polymer volume composition f_A and the segregation strength χN, where χ is the effective A/B segment interaction parameter that depends inversely on temperature and N is the degree of polymerization. Generally, block copolymer microphase separation occurs when the value of χN exceeds a critical composition- and architecture-dependent value [11,14].

Beyond the lamellar (smectic) phases that self-assemble at nearly symmetric compositions $f_A \approx f_B$, A/B block copolymers with asymmetric compositions form ordered two-dimensional (2D) columnar, three-dimensional (3D) network, and 3D spherical micelle packings [8,15–17]. These non-lamellar phases exhibit varying degrees of frustrated space filling, which is minimized by the selection of specific ordered-state symmetries [18,19]. In the case of columnar packings, the preference for 2D hexagonally packed cylinder (HEX) morphologies arises from the fact that the hexagonal Wigner-Seitz cells of this lattice most closely approximate the preferred circular cross-section of a cylinder, while allowing 2D plane tessellation without costly density fluctuations due to loss of van der Waals cohesion in the copolymer melt [15,20].

Until relatively recently, the high-symmetry, body-centered cubic (BCC) spheres morphology was thought to be the only stable micelle packing in microphase separated AB diblock copolymers [6,11]. This structure also exhibits packing frustration due to the preferred local spherical particle symmetry, which must be broken to conform with the truncated cuboctahedral Wigner-Seitz cells of the underlying lattice that tesselate 3D space [21]. Lee *et al.* [16] reported the discovery of a Frank-Kasper (FK) σ phase, with a giant tetragonal unit cell comprising 30 block copolymer micelles of five symmetry-equivalent classes, each with discrete numbers of chains per micelle and average lattice coordination numbers $(CN)_{avg} > 13$ (Fig. 1). In subsequent experiments, Lee *et al.* [18] and, in theory, Reddy *et al.* [22] rationalized the

*Author to whom correspondence should be addressed: maheshkm@umn.edu, he/him/his

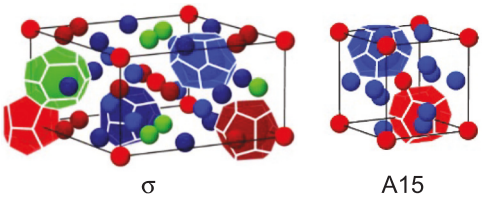

FIG. 1. Unit cells of tetrahedrally close-packed, Frank-Kasper (FK) σ and A15 phases observed in AB diblock copolymers. The lattice Wigner-Seitz cells, which are depicted as colored polyhedra in each rendering, highlight the presence of $\geqslant 2$ classes of symmetry-equivalent micelles with different particle volumes that are characteristic of these FK phases.

formation of the σ phase as a 3D tessellation of space that maximizes van der Waals cohesion at the particle ensemble (unit cell) length scale, while maximizing the local spherical character of each particle with minimal interfacial area. Emergence of this complex phase crucially relies on the ability of the micelles to reconfigure their sizes through interparticle chain exchange to minimize ensemble free energy [18,23]. This dynamic reconfigurability of block copolymer micelles crucially differentiates these systems from high-symmetry face-centered cubic (FCC) and hexagonal close-packed (HCP) crystals of immutable hard sphere colloids [24]. Since this discovery, a variety of tetrahedrally close-packed (TCP) FK phases have been experimentally discovered in diblock polymers, including the A15 phase [25] (Fig. 1), related dodecagonal quasicrystals (DDQCs) [26–28], and C14 and C15 Laves phases [17,29]. Each of these structures is characterized by a unit cell comprising $\geqslant 2$ classes of symmetry-equivalent particles of discrete sizes that occupy different coordination environments.

The role of molecular architecture in complex FK phase stabilization has more recently captured the attention of various groups. Building on initial theoretical work by Grason and Kamien [30], Xie *et al.* [31] used self-consistent mean-field theory (SCFT) to predict that AB_n miktoarm copolymers [Fig. 2(a)] would display wide micellar FK phase windows. These predictions are borne out in recent reports [32,33]. Additionally, Barbon *et al.* [34] reported that conformationally asymmetric and narrow dispersity AB diblock, ABA triblock, and $(AB)_n$ ($n = 3, 4$) core-shell star polymers linked through the majority B segment at a pointlike (zero-dimensional) junction with $f_A = 0.20$–0.35 also form FK A15 and σ phases [Fig. 2(b)]. By synthesizing these various block copolymer architecture analogs so that their constituent AB diblock units had similar N values, Barbon *et al.* [34] quantitatively compared the stabilities of these TCP phases. Notably, they found that the A15 and σ windows for the ABA triblocks were the largest among the examined architectures. The ability of other block copolymer architectures to support or suppress the formation of these complex micellar phases is otherwise relatively untested.

Herein, we address the ability of an A/B core-shell bottlebrush (csBB) copolymer architecture [Fig. 2(c)] to form low-symmetry FK micelle packings. We first describe the synthesis of three relatively narrow dispersity polylactide-*block*-poly(ε-decalactone)-*block*-polylactide (LDL) triblock

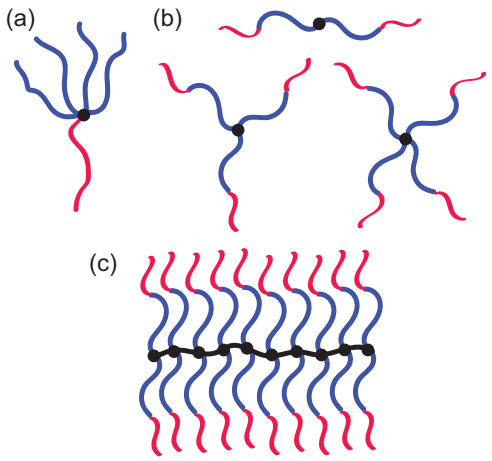

FIG. 2. Block copolymer architectures that support the formation of Frank-Kasper (FK) phases, including (a) AB_n miktoarm stars, (b) $(AB)_n$ core-shell star polymers ($n = 2 - 4$), and (c) the core-shell bottlebrush polymers that are considered in this paper.

copolymers bearing a midchain norbornyl unit with asymmetric polylactide volume compositions $f_L \approx 0.30$. Variable-temperature small-angle x-ray scattering (VT-SAXS) analyses of the LDL triblock morphologies demonstrate that they form equilibrium σ and A15 phases as well as metastable DDQCs that exhibit marked sample processing history dependences. Using living ring-opening metathesis polymerization (ROMP) of the midchain norbornene unit in each of these LDL triblocks, we also synthesize well-defined csBB polymers and show that the stabilities of the FK sphere packings relative to the HEX phase depend on the bottlebrush backbone degree of polymerization (N_{bb}).

II. LDL TRIBLOCK COPOLYMER SYNTHESES AND PHASE BEHAVIORS

By the previously reported Sn-catalyzed, sequential ring-opening transesterification polymerization (ROTEP) sequence [35] depicted in Fig. 3, we synthesized three LDL triblock copolymers with asymmetric poly(lactide) volume fractions. More explicitly, use of a difunctional 5-norbornene-exo-exo-2,3-dimethanol initiator enables bidirectional syntheses of LDL polymers with total molecular weights $M_n = 16.0$–18.1 kg/mol and relatively narrow molar mass dispersities $f_L = 0.27-0.31$, which bear a polymerizable norbornene functionality situated at each chain midpoint. This functionality can be used to enchain these macromonomers into bottlebrush copolymers, as later described (see Fig. 3 and Sec. III). Representative size-exclusion chromatography (SEC) and ^{1}H nuclear magnetic resonance (NMR) data for a representative D homopolymer and LDL triblock are given in Supplemental Material Figs. S1–S3 [36]. These samples are hereafter identified as LDL(N_{total}, f_L), where N_{total} is the total number-average degree of polymerization calculated relative to the 118 Å^3 volume with the melt homopolymer densities, $\rho_D = 0.97$ g/cm^3, and $\rho_L = 1.24$ g/cm^3 at 25 °C [37,38]. The molecular characteristics of these samples are given in Table I.

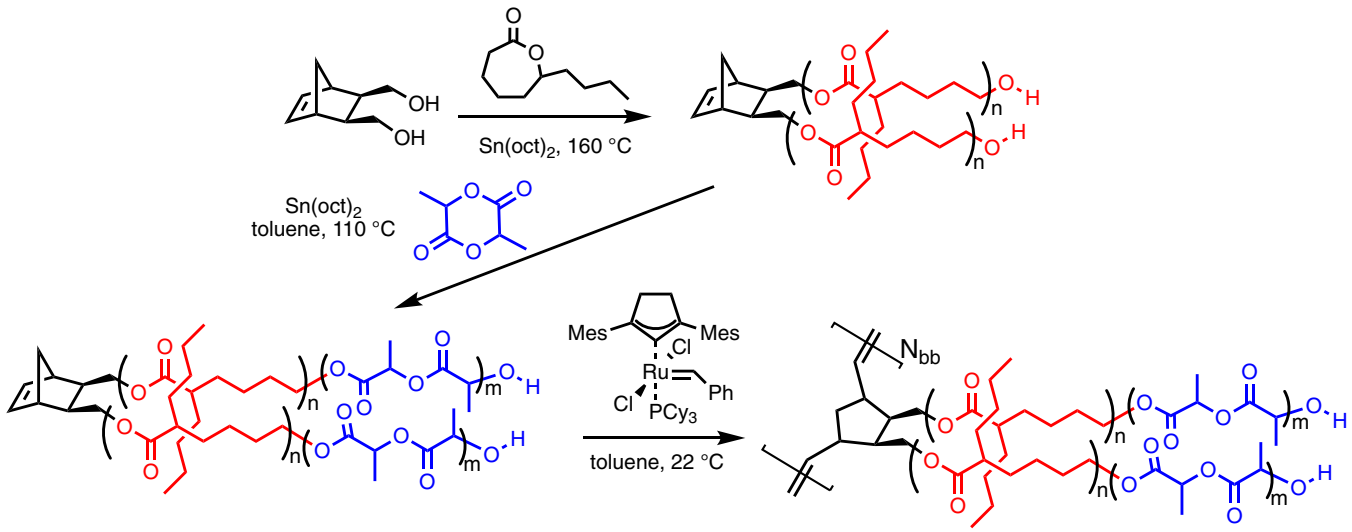

FIG. 3. Sn-catalyzed, controlled and bidirectional synthesis of LDL triblock copolymers from 5-norbornene-exo-exo-2,3-dimethanol and derivative csLDL bottlebrushes.

We studied the microphase separated morphologies of the LDL triblock copolymers by synchrotron VT-SAXS at the Advanced Photon Source (APS, Argonne, IL). By virtue of limited synchrotron beamtime, we performed *ex situ* analyses of the copolymer morphologies by an adaptation of the method of Chang and Bates [28]. More specifically, LDL triblocks were dissolved in toluene and solvent cast at 90 °C into aluminum differential scanning calorimetry pans, followed by heating to 130 °C *in vacuo* for 2 h to effect solvent removal (see Supplemental Material [36] for details). Samples were then hermetically sealed to minimize oxidative degradation during subsequent thermal annealing and SAXS analyses. Five samples of each LDL triblock were prepared and thermally annealed for 12 h at each of five selected temperatures $90 \leqslant T \leqslant 140$ °C using a temperature-regulated hotplate (±3 °C temperature stability), followed by quenching in liquid nitrogen to preserve the melt morphology by rapid vitrification of the minority L domains ($T_{g,L} = 55$ °C) and the majority D domains ($T_{g,D} = -51$ °C) to lock in the high-temperature structure [39,40]. Samples were removed from the $N_2(l)$ bath and allowed to warm to 25 °C for SAXS analyses.

Representative azimuthally integrated SAXS patterns obtained at 25 °C arising from this sample processing protocol are displayed in Fig. 4. LDL(215,0.28) samples annealed either at 90 or 100 °C yield powder diffraction signatures of a micellar DDQC that comprise a sharp, low-q peak and three broader, closely spaced peaks at higher q values [Fig. 4(a)] [26]. The low-$q = 0.0348$ Å^{-1} peak corresponds to the periodic interplanar spacing $d_{(00002)} = c/2 = 18.1$ nm between the layers of aperiodically arranged micelles in this axial 12-fold quasicrystal. Using the five-dimensional indexing scheme developed for intermetallic DDQCs [41,42] that has been applied to structurally analogous micellar soft materials [26,27], we conclude that the micelle center-to-center distance in the planes of aperiodically ordered particles is $a = 35.6$ nm with $c/a = 1.017$ [27]. Annealing this polymer at 110 °C instead yields SAXS patterns with substantially textured powder diffraction rings indicative of large grain sizes [Fig. 4(a), inset], which slightly broaden the peaks in the 1D-SAXS intensity profile in Fig. 4(a). This unique scattering signature corresponds to a translationally periodic FK σ phase with $P4_2/mnm$ symmetry, with tetragonal lattice parameters $a = 67.7$ nm and $c = 35.9$ nm with $c/a = 0.530$ that is close to the ideal value of 0.526 [16,18]. The close correspondence of the interplanar $d_{(00002)}$ spacing in the DDQC and that of its σ approximant $d_{(002)} = c/2 = 18.0$ nm is in accord with prior reports of diblock copolymer quasicrystals [26,28]. Finally,

TABLE I. Molecular characteristics of LDL triblock polymers.

LDL(N_{tot}, f_L)	$M_{n,D}$[a] (kg/mol)	$Đ_D$[b]	$M_{n,L}$[a] (kg/mol)	$Đ_{LDL}$[b]	N_{tot}[c]	f_L[c]	T_{ODT}(°C)[d]
LDL(245,0.27)	12.3	1.19	2.9	1.22	245	0.27	140
LDL(215,0.28)	10.6	1.17	2.7	1.20	215	0.28	125
LDL(218,0.31)	10.4	1.21	3.0	1.21	218	0.31	135

[a]Determined using ^{1}H NMR endgroup analysis per spectra in Figs. S1 and S2 in the Supplemental Material [36].
[b]Determined by SEC against narrow dispersity polystyrene standards in THF at 22 °C.
[c]N_{tot} is the total segment-density normalized degree of polymerization relative to the 118 Å^3 reference volume and f_L is the polylactide volume fraction, which were calculated using the homopolymer densities $\rho_D = 0.97$ g/cm^3 and $\rho_L = 1.24$ g/cm^3 at 25 °C.
[d]Measured by VT-SAXS with a temperature resolution $\Delta T = 3$ °C on heating, using samples prepared by annealing at T_{anneal} for 12 h and prior to quenching in $N_2(l)$: $T_{anneal} = 127$ °C for LDL(245,0.27), 110 °C for LDL(215,0.28), and 100 °C LDL(218,0.31).

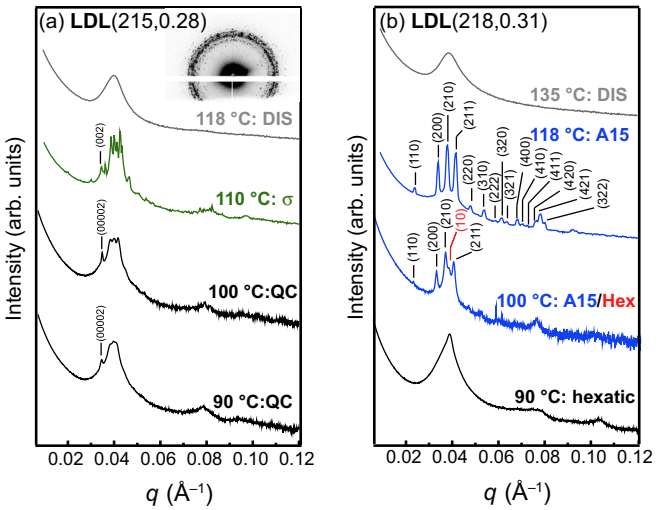

FIG. 4. Azimuthally averaged one-dimensional (1D) small-angle x-ray scattering (SAXS) intensity profiles for (a) LDL(215,0.28) and (b) LDL(218,0.31) acquired at 25 °C, after isothermal annealing for 12 h at the indicated temperatures, quenching in liquid nitrogen, and rewarming to ambient temperature. Peak broadening recorded in the intensity profile for LDL(215,0.28) annealed at 110 °C stems from the textured nature of the two-dimensional (2D)-SAXS pattern [panel (a) inset].

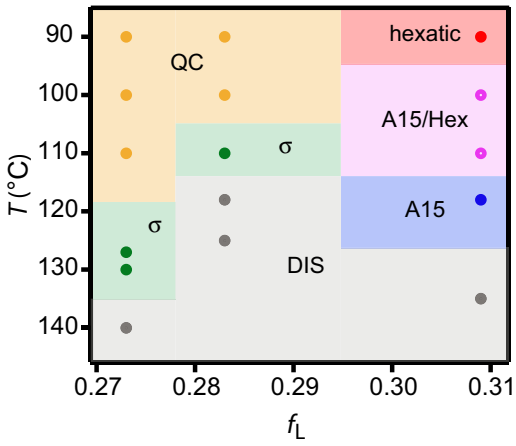

FIG. 5. Morphology diagram based on ex situ small-angle x-ray scattering (SAXS) analyses at 25 °C of LDL(245,0.27), LDL(215,0.28), and LDL(218,0.31) after thermal annealing at the indicated temperatures.

the SAXS patterns for samples annealed at $T \geqslant 118$ °C yield only a single broad, low-intensity peak, consistent with the correlation-hole scattering of a fluctuating, disordered micellar melt [43,44].

The *ex situ* annealing temperature-dependent sequence of phases depends sensitively on the triblock copolymer composition, per data in Fig. 4(b) for LDL(218,0.31) with a slightly higher f_L value. SAXS analysis of a sample preannealed at 90 °C revealed a broad yet high-intensity primary peak with two broad, higher-order scattering maxima. This scattering signature is possibly indicative of a poorly ordered yet microphase-separated morphology with hexatic order, evidenced by broad SAXS maxima at $(q/q*)^2 \approx 1, 4, 7$ ($q* = 0.0397$ Å^{-1}). Increasing the sample preannealing temperature to 100 °C drives its ordering into a cubic FK A15 phase with $Pm\bar{3}\ n$ symmetry, for which the cubic unit cell parameter $a = 38.1$ nm with characteristic SAXS peaks at $(q/q*)^2 = 2$, 4, 5, 6, etc. [25,45]. We note that the (210) peak exhibits a high-q shoulder due to the coexistence of another morphology. We resolved the identity of this coexisting phase as HEX, by heating the sample preannealed at 90 to 110 °C and observing that it transiently yields a SAXS signature with characteristic peaks at $(q/q*)^2 = 1, 4$, and 7 for which the $q*$ peak coincides with the location of the shoulder on the A15 (210) peak; after a 10 min thermal equilibration time, SAXS analyses furnish a pattern like that in Fig. 4(b) at 100 °C. The emergence of a transient HEX phase from the lower-temperature hexatic structure is also consistent with this assignment. A15/HEX coexistence is not unexpected given that these morphologies often form proximally in phase space [25,46,47]. While two-phase coexistence is forbidden by the Gibbs phase rule for a one-component system at equilibrium, the molecular weight dispersity of this sample ($Đ_{LDL} = 1.21$) formally implies that this sample comprises multiple molecular species, thus relaxing this criterion. However, this coexistence could also arise from phase transformation kinetics that are slow even at the 12 h time scale of the sample preannealing, given the minute free energy difference between the HEX and A15 phases in diblock copolymers [17] and the slow chain diffusion in such segregated melts [48,49]. We return to this point below when considering temperature-dependent SAXS analyses of samples preannealed at different temperatures. Preannealing LDL(218,0.31) at 118 °C yields a pure A15 phase, while a disordered micellar melt is formed by the sample preannealed at 135 °C.

Results of the *ex situ* thermal annealing studies for the three LDL triblocks are graphically summarized in Fig. 5. Gillard *et al.* [26] and Mueller *et al.* [27] previously demonstrated the path-dependent formation of block copolymer DDQCs by rapid thermal quenching of disordered particle-forming diblock melts to form nonergodic micelle glasses, followed by isothermal annealing at lower temperatures. These micelle glasses or liquidlike packings (LLPs) of micelles are thought to comprise broad and continuous distributions of particle sizes [50]. Since intermicellar block copolymer chain exchange is a thermally activated process, the micelle size distribution reconfigures very slowly at lower temperatures and short annealing times, thus disallowing formation of the discrete micelle size distributions required for σ and A15 structure formation [18]. However, the limited micelle mobility conferred by low-temperature annealing apparently enables low-barrier nucleation and growth of nonequilibrium, aperiodically ordered DDQCs, which ultimately transform into equilibrium FK σ phases after extended annealing or on heating [27]. DDQC formation in LDL(215,0.28) is consistent with these ideas since the sample thermal history involved initial heating to 130 °C to access a disordered micellar melt, followed by cooling to 25 °C. This thermal history traps a micellar LLP. Subsequent sample preannealing at 90 or 100 °C furnishes sufficient micelle mobility to nucleate and grow a DDQC. However, the kinetics of interparticle chain exchange

required to form the discrete micelle size distribution for periodic FK phase formation are slow at 90 and 100 °C on the 12 h sample preannealing time scale. Heating this sample to 110 °C instead facilitates faster chain exchange over 12 h, thereby facilitating σ-phase formation with large grain sizes. Consistent with this line of reasoning is the observation that the σ phase often forms at higher temperatures in copolymers that form DDQCs at low temperatures [27]. LDL(245,0.27) also forms DDQCs after initial sample processing and 12 h preannealing steps at $T \leqslant 110$ °C. In this case, we speculate that sample solvent casting from toluene yields a segregated, nonequilibrium LLP that persists through solvent removal at 130 °C for 2 h and subsequent cooling to ambient temperature (note that the sample is ordered at 130 °C per Fig. 5). This LLP again nucleates a DDQC on melt annealing for 12 h at $T \leqslant 110$ °C; however, faster intermicellar chain exchange at $T > 110$ °C enables σ-phase formation. Since the rate of interparticle chain exchange in a block copolymer melt scales as $\exp(-\chi N)$ [51,52], we calculated the χN values for σ-phase-forming melts using the reported L/D segment effective interaction parameter $\chi(T) = (97.0/T) - 0.138$ referenced to the 118 Å^3 segment volume [35]. This calculation reveals that the segregation strengths of LDL(245,0.27) annealed at 127 °C and LDL(215,0.28) annealed at 110 °C are comparable with $\chi N = 24.8$–25.6, further supporting the notion that micelle size distribution reconfiguration is essential for σ-phase formation. On the other hand, LDL(218,0.31) displays no such nonequilibrium phase behavior, possibly due to the fact that the FK A15 phase with a discrete micelle size distribution can form directly by fission of HEX micelles that form at low temperatures. Thus, this morphological transition obviates the need for micelle size equilibration by chain exchange in the segregated point particle packing.

Toward our goal of understanding how enchaining LDL triblock macromonomers into csBBs influences both their morphologies and self-assembly thermodynamics, we determined the order-to-disorder transition temperature (T_{ODT}) for each sample in Table I. VT-SAXS measurements (see Supplemental Material [36] for details) offer a convenient means for determining T_{ODT}, which is identified as the temperature at which the sharp Bragg scattering peaks of an ordered morphology are replaced by the broad, correlation-hole scattering of a disordered melt [43]. After *ex situ* sample preannealing at 110 °C into a σ phase with large grain sizes (*vide supra*), VT-SAXS patterns acquired on heating LDL(215,0.28) show that $T_{ODT} = 125 \pm 3$ °C (Fig. 6). Significant texture in the diffraction pattern reported at 25 °C results in a slightly unusual 1D-SAXS intensity profile, while the pattern acquired at 80 °C apparently reflects somewhat reduced σ-phase order due to structure rearrangement associated with L domain mobility ($T_{g,L} \approx 55$ °C). Note that the stated uncertainty in T_{ODT} stems from the $\Delta T = 3$ °C resolution of our measurements. Temperature-dependent SAXS patterns for LDL(245,0.27) preannealed at 127 °C into a σ phase indicate only modest lattice parameter changes (<1.5%) on heating with no order-to-order phase transitions up to $T_{ODT} = 140 \pm 3$ °C. On the other hand, the observed T_{ODT} by SAXS for LDL(218,0.31) depends on the *ex situ* sample annealing temperature. In heating ramps starting at 25 °C, the A15/HEX coexistence derived by preannealing LDL(218,0.31) at 110 °C yielded the

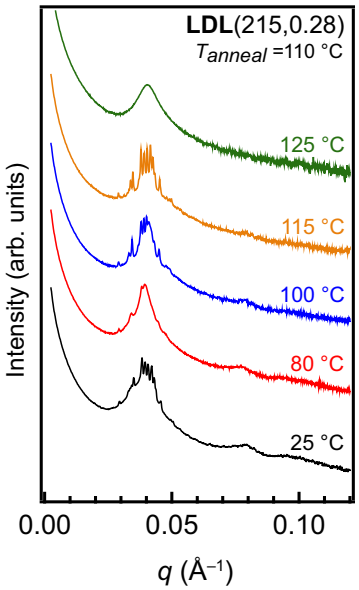

FIG. 6. One-dimensional (1D) small-angle x-ray scattering (SAXS) profiles for σ phase-forming LDL(215,0.28) on heating, after isothermal annealing at 110 °C for 12 h, indicate that $T_{ODT} = 125$ °C.

following phase sequence:

$$\text{A15/HEX}(118\,^\circ\text{C}) \rightarrow \text{A15/HEX}(122\,^\circ\text{C}) \rightarrow \text{A15/disorder}\ (135\,^\circ\text{C}) \rightarrow \text{disorder},$$

with $T_{ODT} = 135 \pm 3$ °C, where the parenthetical values indicate the phase transition temperatures. If one instead preanneals this sample at 118 °C into a pure A15 phase and quenches it to trap this high-temperature morphology, the observed phase progression on heating from 25 °C is instead

$$\text{A15}(63\,^\circ\text{C}) \rightarrow \text{A15/HEX}(129\,^\circ\text{C}) \rightarrow \text{disorder},$$

with $T_{ODT} = 129 \pm 3$ °C and no pure A15 phase observed when $T > T_{g,L}$. Note that this starting A15 phase observed at 25 °C is kinetically trapped by liquid nitrogen quenching of the sample annealed at 118 °C. The pure A15 phase reversion to A15/HEX coexistence at 63 °C, just above $T_{g,L} = 55$ °C when the L segments devitrify, suggests that the HEX phase noted in Fig. 4(b) at 90 °C is likely an equilibrium structure possibly with an intervening window of A15/HEX. That this coexistence persists up to T_{ODT} is likely a consequence of the slow kinetics of HEX/A15 phase conversion into pure A15 on the ~3 h time scale of this VT-SAXS heating ramp as compared with the *ex situ* 12 h annealing result described above. Consequently, we assign A15 as the equilibrium high-temperature phase with its higher T_{ODT} value for this sample.

III. csBB PHASE BEHAVIOR

We used living ROMP catalyzed by a Grubbs third-generation ruthenium catalyst to enchain the reactive norbornene functionalities at the LDL triblock chain midpoints into csBB polymers [35] with backbone degrees of polymerization $N_{bb} = 5$–49 (Fig. 3). In all cases, SEC using multi-angle laser light scattering (SEC-MALLS) detection yielded

TABLE II. Molecular characteristics of asymmetric csLDL block polymer bottlebrushes.

csBB	$M_{n,\mathrm{csLDL}}$	$Đ_{\mathrm{csLDL}}$[a]	T_{anneal}(°C)[b]	Morphology[c]	T_{ODT}(°C)[d]	$(\chi N_{\mathrm{arm}})_{\mathrm{ODT}}$[e]
LDL(215,0.28)	16.1	1.20	110	$\sigma \rightarrow$ Dis	116	23.9
csLDL(215,0.28)–5	75.8	1.09	110	A15 $\rightarrow$ Dis	134	21.6
csLDL(215,0.28)–9	149	1.05	110	A15/HEX $\rightarrow$ Dis	139	20.9
csLDL(215,0.28)–21	345	1.07	110	HEX/A15 $\rightarrow$ Dis	151	19.5
csLDL(215,0.28)–36	588	1.07	110	HEX $\rightarrow$ Dis	156	18.9
LDL(218,0.31)	18.3	1.21	114	A15$\rightarrow$A15/HEX$\rightarrow$A15$\rightarrow$Dis	135	23.1
csLDL(218,0.31)–4	80.8	1.09	114	HEX/A15 $\rightarrow$ Dis	142	20.8
csLDL(218,0.31)–8	145	1.03	114	HEX/A15 $\rightarrow$ Dis	154	19.4
csLDL(218,0.31)–26	481	1.05	114	HEX $\rightarrow$ Dis	>170	–
csLDL(218,0.31)–49	907	1.11	114	HEX $\rightarrow$ Dis	161	18.7

[a]Determined by SEC in THF at 22 °C against PS standards.
[b]Samples were preannealed at the listed temperature for 12 h and immediately quenched in liquid nitrogen to vitrify the sample.
[c]Morphology determined from by SAXS on heating from 25 °C after *ex situ* thermal preannealing and quenching.
[d]T_{ODT} measured by VT-SAXS with a temperature resolution $\Delta T = 3$ °C.
[e]$(\chi N_{\mathrm{arm}})_{\mathrm{ODT}}$ calculated using the reported $\chi(T) = 97/T - 0.138$ of the L/D monomer pair [35].

dispersities $Đ \leqslant 1.10$ in a manner consistent with the prior literature on which our synthetic approach is based [53–55]. However, we report the csBB dispersities $Đ \leqslant 1.11$ in Table II measured by SEC using narrow dispersity polystyrene standards for comparison and consistency with the values reported for the lower-molecular-weight LDL macromonomers (Table I). Since we specifically sought to understand how this nonlinear block copolymer brush architecture impacts the stabilities of σ and A15 phases as a function of N_{bb}, we focused our attention on two csBB series derived from σ- and A15-forming LDL(215,0.28) and LDL(218,0.31), respectively. Molecular characteristics of the two macromonomers and eight daughter bottlebrushes are given in Table II. Brush backbone degree of polymerization values were experimentally determined as $N_{\mathrm{bb}} = M_{n,\mathrm{csLDL}}/M_{n,\mathrm{LDL}}$, where $M_{n,\mathrm{csLDL}}$ was determined by SEC-MALLS and $M_{n,\mathrm{LDL}} = M_{n,\mathrm{D}} + 2M_{n,\mathrm{L}}$ was calculated from Table I (see Supplemental Material [36] for experimental conditions). We hereafter identify these samples as csLDL(N_{arm}, f_{L})–N_{bb}, where N_{arm} is the LDL triblock macromonomer volume-referenced degree of polymerization and N_{bb} is the backbone chemical degree of polymerization.

Samples were pretreated by the *ex situ* thermal annealing procedure using the temperatures listed in Table II, prior to morphological analyses on first heating by VT-SAXS. Representative 1D-SAXS intensity profiles for the LDL macromonomers and daughter csBBs are presented in Fig. 7. At 25 °C, the csLDL(215,0.28) series exhibits the phase sequence [Fig. 7(a)]:

$$\sigma(1) \rightarrow \mathrm{A15}(9) \rightarrow \mathrm{A15/HEX}(36) \rightarrow \mathrm{HEX},$$

where the parenthetical values are the N_{bb} values at which architecture-induced phase transitions are observed within the resolution of our measurements. We find no evidence for DDQC formation in these csBBs. The HEX phases are characterized by intense SAXS peaks located at $(q/q*)^2 = 1$, 3, and 7 with $q* = 0.038$–0.041 Å, corresponding to cylinder center-to-center distances 17.7–18.6 nm that increase slightly as N_{bb} increases. In samples assigned as A15/HEX coexistence (e.g., Fig. 7, $N_{\mathrm{bb}} = 9$ and 21), we typically observe broadening of the (211) reflection of the A15 phase [see Fig. 4(b) for representative SAXS pattern indexing] due to its near coincidence with the $q*$ peak of the HEX morphology corresponding to its (10) reflection. In lyotropic liquid crystal assemblies of ionic small molecule surfactants, Perroni and Mahanthappa [47] have previously reported a similar structural relationship in samples exhibiting A15/HEX phase coexistence. Note that polymerization of the norbornene functionality at the LDL triblock chain midpoint places the csBB backbone in the D matrix domain, while the minority L segments form the micelle cores in these microphase separated structures. On heating these samples to 110 and 132 °C, we observed the retention of these phases albeit with sharpening of the peaks [Figs. 7(b) and 7(c)]. The lattice parameter for the A15 phase $a = 35.5$ nm remains invariant (within 1%) with N_{bb} in melts analyzed at 110 °C; furthermore, the near coincidence of the σ $d_{(002)} = 18.0$ ($N_{\mathrm{bb}} = 1$) and the A15 $d_{(200)} = 17.8$ nm ($N_{\mathrm{bb}} = 5$, 9, 21) is expected based on similarities in the layered structures of these FK phases [26,27].

The csLDL(218,0.309) series exhibits a similar sequence of order-to-order transitions [Figs. 7(d)–7(f)]:

$$\mathrm{A15}(1) \rightarrow \mathrm{HEX/A15}(26) \rightarrow \mathrm{HEX},$$

on increasing N_{bb} from 1 to 49, albeit with a ~3.5% decrease in the A15 lattice parameter on csBB backbone elongation ($a = 36.8$ nm at 110 °C for $N_{\mathrm{bb}} = 8$). This contraction in the A15 lattice parameter may reflect reductions in the LDL intermolecular distances imposed by covalently linking their midpoints into csBBs; a similar degree of domain size contraction was previously reported in csBB lamellar phases with $f_{\mathrm{L}} \approx f_{\mathrm{D}}$ [35]. These two datasets unequivocally demonstrate that the stability of complex micellar phases in A/B block copolymers depend on molecular architecture. More specifically, the csBB structure drives transitions to morphologies with lower interfacial curvatures as N_{bb} increases, with a preference for forming HEX phases at the longest backbone lengths.

We also determined T_{ODT} for each sample by SAXS on heating per the methodology described above for the parent LDL triblocks. Attendant with the N_{bb} dependence of the observed morphology, we found that T_{ODT} increases with increasing N_{bb}. Table II lists the T_{ODT} values for each csBB, and the observed ordered phase sequences determined by

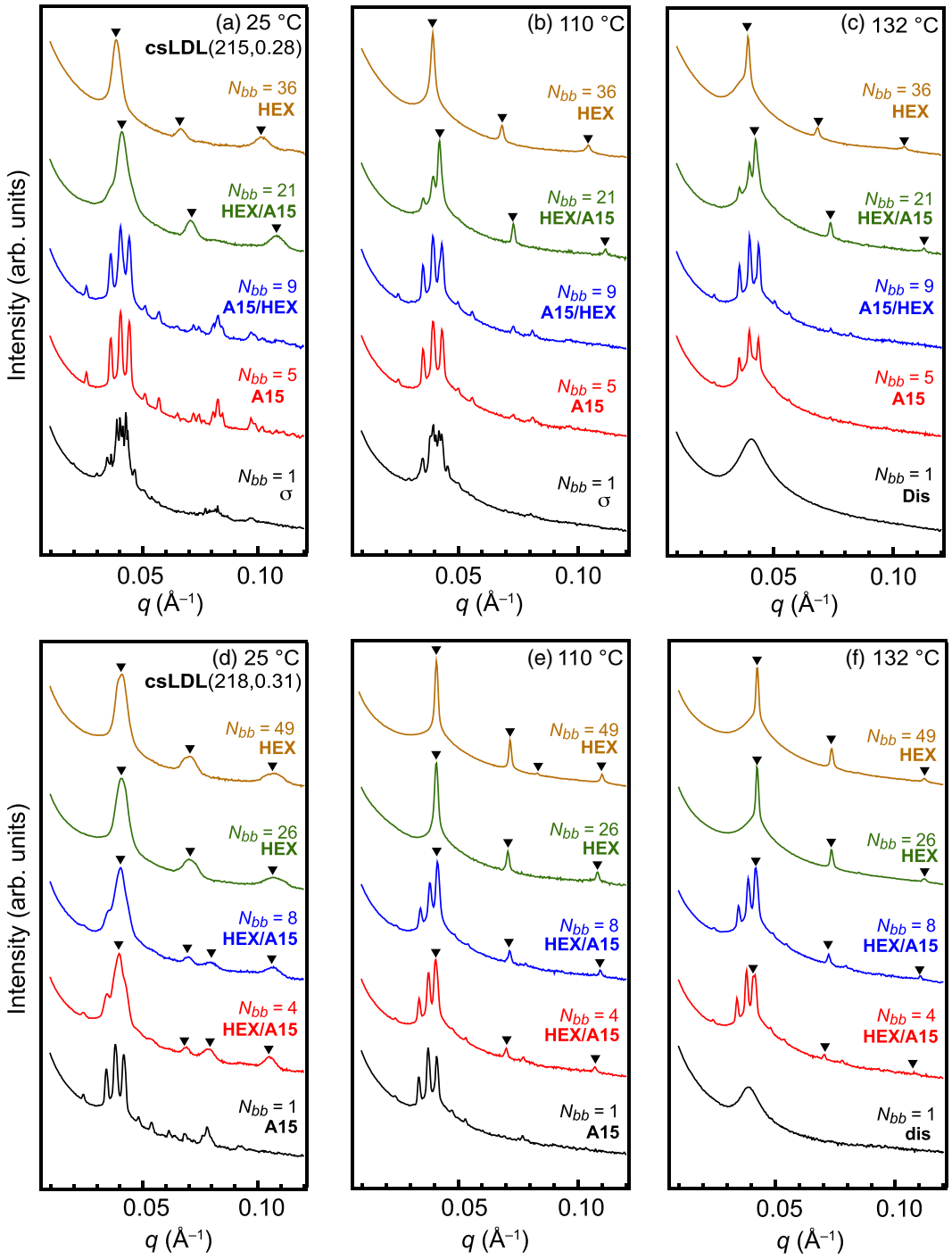

FIG. 7. One-dimensional (1D) small-angle x-ray scattering (SAXS) intensity profiles for core-shell bottlebrushes (csBBs) acquired at the indicates temperatures: (a)–(c) csLDL(215,0.28) and (d)–(f) csLDL(218,0.31). Data have been vertically shifted for clarity, and peak markers indicate the positions of SAXS peaks associated with hexagonally packed cylinder (HEX) phases.

SAXS on heating. We did not pursue syntheses of csBBs based on LDL(245,0.27) with $T_{ODT} = 140\,^{\circ}C$ since bottlebrushes derived therefrom were expected to exhibit T_{ODT} values exceeding the sample decomposition onset temperature ($T_{decomp} \approx 170\,^{\circ}C$). The data show that T_{ODT} increases by 6% in absolute temperature from 116 to 139 °C on enchaining LDL(215,0.28) into a csBB with $N_{bb} = 9$ (Table II) with a change in morphology from σ to A15. However, a somewhat smaller increase $\Delta T_{ODT} = 17\,^{\circ}C$ occurs on bottlebrush chain extension from $N_{bb} = 9$ to 36, again with a morphology change from A15 to HEX. Similarly, T_{ODT} for csLDL(218,0.31)–9 is 7% higher in absolute temperature than that of the parent LDL triblock. For csLDL(218,0.31)–26, VT-SAXS experiments yielded $T_{ODT} > T_{decomp} \approx 170\,^{\circ}C$. This result is somewhat anomalous in light of the smaller T_{ODT} increases noted in the csLDL(215,0.28) series as a function of N_{bb}, and related monotonic increases in T_{ODT} observed in lamellar csBBs with increasing N_{bb} [35]. We ascribe this

unexpected result to the somewhat broader backbone dispersity of the csLDL(218,0.31)–26, whereby chains with longer backbones thermally stabilize the ordered morphology. Since the morphologies of the csBBs change with increasing N_{bb}, we forgo quantitative assessment of how the value of $(\chi N_{LDL})_{ODT}$ varies with N_{bb} in this region of composition space. However, we do note that the HEX phases formed at the largest N_{bb} values apparently exhibit a limiting value of $(\chi N_{arm})_{ODT} \approx$ 18.7–18.9.

IV. DISCUSSION

We first consider reasons for the somewhat surprising emergence of TCP FK σ and A15 phases and related DDQCs in LDL triblock copolymers. SCFT calculations by Xie *et al.* [31] predicted the stability of micellar FK phases in AB-type diblock copolymers with high degrees of conformational asymmetry. Conformational asymmetry, which is defined as $\varepsilon = (b_A/b_B)^2 > 1$ where the b_i's are the volume-referenced statistical segment lengths of the constituent blocks, quantifies the unequal entropy penalties for segment stretching in the constituent blocks that are proportional to $(1/b_i)^2$ [56,57]. Sphere-forming diblocks with $f_A < 0.5$ and $b_A > b_B$ are thus expected to form FK phases. This scenario physically translates into the micelle corona B segment being less extensible than the core A segment, so that the micelle strongly prefers spherical particle symmetry [27]. This limited corona extensibility consequently drives packing frustration in ordered diblock copolymer melts comprising spherical micelles, wherein the chains must fill space at constant density to maximize van der Waals cohesion in the particle ensemble. Reddy *et al.* [22] have established how simultaneous maximization of van der Waals cohesion in the particle ensemble and local spherical particle symmetry with minimal interfacial area drives spontaneous symmetry breaking to form low-symmetry FK phases.

Based on qualitative correlations between monomer molecular structure and statistical segment length [57–59], we speculated that the stability of FK phases in LDL triblocks stems from the conformational asymmetry of this monomer pair. While the statistical segment length of L is known to be $b_L = 7.9$ Å relative to the 118 Å^3 reference volume [37], a b value for D has not been reported. Consequently, we used the apparently universal packing length correlation of Fetters *et al.* [58,59] with the entanglement molecular weight $M_e = 5.9$ kg/mol for D measured by Martello *et al.* [38] to estimate $b_D = 6.0$ Å relative to the common reference volume (see Supplemental Material [36] for the detailed calculation). Thus, we estimate $\varepsilon = (b_L/b_D)^2 = 1.7$, which suggests that the LDL triblock copolymers are conformationally asymmetric and expected to form FK phases as in our experiments. As noted previously by Barbon *et al.* [34], this conformational asymmetry is apparently large enough to overcome the expected preference for curvature toward the center D segments of LDL triblocks, which arises from their architectural asymmetry that skews the morphology diagram for ABA-type triblocks [10,11]. In fact, the observed volume fraction of the FK σ and A15 phase windows in this paper nearly quantitatively agree with those reported previously by Zhang *et al.* [60] for $FA_{12}F$ triblock copolymers [F = poly(2,2,2-trifluoroethyl acrylate) and A_{12}= poly(2-dodecyl acrylate)] with $\varepsilon = (b_F/b_{D12})^2 = 2.04$. Furthermore, the segregation strengths of the three LDL triblock copolymers reported here at the order-disorder transition temperature are $22 \leqslant (\chi N)_{ODT} \leqslant 24$. These values closely agree with those reported for even narrower dispersity $FA_{12}F$ triblocks with experimentally measured overall molar mass dispersities $\leqslant$1.13 [60]. These observations demonstrate that the LDL triblock copolymer molar mass dispersities ($\leqslant$ 1.22 in Table I) do not appreciably alter their microphase separation behaviors anticipated by their conformational asymmetry. We do, however, note that recent theories [61] and related copolymer blending experiments [62–64] suggest that broadening copolymer molar mass dispersities can sometimes stabilize FK phases.

In experimental studies, Lewis *et al.* [65] have suggested that FK phases only form in low-molar-mass diblocks with invariant degrees of polymerization $\bar{N}_{diblock} = Nb^6/v^2 \lesssim 600$, where b is the statistical segment length associated with the $v = 118$ Å^3 reference volume. Calculation of the $\bar{N}$ values as the sum of the values for each segment in the LDL triblocks yields $1582 \leqslant \bar{N}_{triblock} \leqslant 1900$. If we consider the triblocks as two covalently end-linked diblocks (e.g., $\bar{N}_{diblock} = \bar{N}_{triblock}/2$), we equivalently find that $791 \leqslant \bar{N}_{diblock} \leqslant 950$. This result differs starkly from the criteria of Lewis *et al.* [65] and suggests that the molecular design rules for conformationally asymmetric triblock copolymers that form micellar FK phases may be different from their diblock analogs. We further note that an absolute error in the value of b_D of >10% would otherwise be required to align the expected $\bar{N}_{diblock}$ with the LDL triblock case.

In the limit of low N_{bb}, one expects csBBs to behave more like core-shell star polymers, because the diblock arms near the short brush backbone ends exhibit significant conformational degrees of freedom (Fig. 2) [66]. Barbon *et al.* [34] previously showed that structurally related $(AB)_n$ ($n = 2 - 4$) core-shell star block copolymers [Fig. 2(b)] with $\varepsilon = 2.04$ thermodynamically self-assemble into FK A15 and σ phases with the star junction located in the matrix domain. The csLDL(215,0.283) series with $N_{bb} \leqslant 9$ similarly support FK phase formation, albeit with a subtle decrease in the mean interfacial curvature that drives a $\sigma \rightarrow$A15 transition. The nearly coincident σ $d_{(002)}$ and A15 $d_{(200)}$ layer spacings in this parent LDL triblock and its daughter csBBs suggest that the underlying molecular packings in these morphologies only subtly differ. However, one must bear in mind that csBBs with $N_{bb} = 5$ each comprise 10 densely grafted DL diblock arms, which probably exhibit highly non-Gaussian chain conformations near the brush backbone [67,68]. We speculate that the conformational restrictions imposed on these densely grafted side chains propagate to the D/L block junctions of each arm to induce a small degree of chain stretching and thus a reduction in the interfacial area per chain, which induces the observed $\sigma \rightarrow$A15 transition. The fact that such a subtle change in chain conformations influences the observed morphology is not surprising, given the small free energy differences between these micellar phases, which are estimated to be $\leqslant 10^{-3}$ kT per diblock chain by SCFT [17,21].

The transition to predominantly HEX morphologies on further lengthening the brush backbone when $N_{bb} \gtrsim 10$ likely

stems from a change in the csBB conformation from a starlike object to a wormlike, cylindrical bottlebrush [Fig. 2(c)]. Levi *et al.* [66] reported a related broad star-to-bottlebrush transition near $N_{bb} \approx 10$ in experiments on brushes with randomly enchained A and B macromonomer arms with $M_n \leqslant 12$ kg/mol and brush backbone dispersities $\leqslant 1.19 - 1.25$ (against linear polystyrene standards), with support from SCFT calculations. We surmise that the conformational restrictions on the DL diblock arms in the cylindrical csBBs, coupled with their crowded packing in the tetrahedral interstitial sites between the micelle cores of the FK phases, destabilizes spherical micelle phases. Instead, a HEX morphology emerges wherein the csBB backbones can alleviate their frustrated packings by aligning the bottlebrush backbones along the long axes of the cylinders. In other words, the axial symmetry of the HEX morphology accommodates the axial symmetry of the shape-persistent cylindrical brush. The formation of HEX morphologies wherein csBBs exhibit local nematic character is consistent with theoretical predictions of the nematic behavior of densely grafted brush homopolymers [69]. We note that the crossover from the starlike regime that stabilizes micellar FK phases to the brush regime that supports the HEX morphology is broad, with significant windows of two-phase coexistence. While the exact origins of these phenomena remain unknown, one possibility is that dispersity in N_{bb} leads to two-phase coexistence due to the presence of both starlike and bottlebrushlike macromolecules in these samples. In accord with this assertion, SAXS analyses in Figs. 7(a)–7(c) reveal that csLDL(215,0.28)–9 is A15 with a minor amount of coexisting HEX, csLDL(215,0.28)–21 is mostly HEX with a small amount of A15, and csLDL(215,0.283)–36 is pure HEX. By analogy to the above case of LDL(218,0.31), an alternative explanation for this coexistence is that the temperature-dependent A15 $\rightarrow$ HEX phase transformation kinetics are slow on the relatively short time scales of the SAXS heating ramps ($\sim$3 h).

In all cases reported here, we note that oligomerization of the LDL triblocks into csBBs results in increases in T_{ODT} with increasing N_{bb}. This trend mirrors our prior finding that oligomerization of compositionally symmetric LDL triblocks into csBBs drives their assembly into lamellar phases with significantly higher T_{ODT} values [35]. The generality with which T_{ODT} increases on oligomerizing both compositionally symmetric and asymmetric ABA-type triblocks into csBBs suggests a common underlying mechanism. More explicitly, linking the triblocks into a csBB decreases the configurational entropy penalty associated with organizing the polymer chains at domain interfaces by preorganizing them for self-assembly.

V. CONCLUDING REMARKS

Synthetic access to complex block copolymer architectures offers exciting opportunities to (de)stabilize specific microphase separated morphologies and to tune their underlying self-assembly thermodynamics. Based on modular macromolecular syntheses, we conducted systematic morphological investigations of the consequences of oligomerizing conformationally asymmetric, relatively narrow dispersity, sphere-forming ABA-type triblock copolymers through a polymerizable midchain functionality into densely grafted csBBs. These studies revealed that the csBB architecture supports micellar FK phase self-assembly when $N_{bb} \lesssim 10$, while HEX phases preferentially form at larger N_{bb} values. These observations suggest the occurrence of a star-to-bottlebrush conformational transition near $N_{bb} \approx 10$. Temperature-dependent SAXS measurements also reveal that the thermal stability of the microphase separated melt increases with increasing N_{bb}, suggesting that the csBB architecture generally reduces the configurational entropy penalty for melt self-assembly.

ACKNOWLEDGMENTS

This paper was funded by National Science Foundation Grant No. DMR-2003668. ^{1}H NMR spectra used in this paper were collected on a Bruker Avance II HD 400 MHz spectrometer purchased by the Office of the Vice President of Research, the College of Science of and Engineering, and the Department of Chemistry at the University of Minnesota. SAXS experiments were carried out at Sectors 12 and 5 of the APS. The Sector 5 DuPont-Northwestern-Dow Collaborative Access Team is supported by E.I. DuPont de Nemours & Co., the Dow, Inc., and Northwestern University. Use of the APS, an Office of Science User Facility operated for the U.S. Department of Energy (DOE) Office of Science by Argonne National Laboratory, was supported by the U.S. Department of Energy under Contract No. DE-AC02-06CH11357.

[1] F. S. Bates and G. H. Fredrickson, Block copolymers—Designer soft materials, Phys. Today **52**(2), 32 (1999).

[2] C. Lang, M. Kumar, and R. J. Hickey, Current status and future directions of self-assembled block copolymer membranes for molecular separations, Soft Matter **17**, 10405 (2021).

[3] S. Kang and M. J. Park, 100th anniversary of macromolecular science viewpoint: Block copolymers with tethered acid groups: Challenges and opportunities, ACS Macro Lett. **9**, 1527 (2020).

[4] A. Alvarez-Fernandez, C. Cummins, M. Saba, U. Steiner, G. Fleury, V. Ponsinet, and S. Guldin, Block copolymer directed metamaterials and metasurfaces for novel optical devices, Adv. Opt. Mater. **9**, 2100175 (2021).

[5] S. Liu, Y. Yang, L. Zhang, J. Xu, and J. Zhu, Recent progress in responsive photonic crystals of block copolymers, J. Mater. Chem. C **8**, 16633 (2020).

[6] L. Leibler, Theory of microphase separation in block copolymers, Macromolecules **13**, 1602 (1980).

[7] L. Wu, E. W. Cochran, T. P. Lodge, and F. S. Bates, Consequences of block number on the order-disorder transition and viscoelastic properties of linear $(AB)_n$ multiblock copolymers, Macromolecules **37**, 3360 (2004).

[8] M. W. Matsen and F. S. Bates, Unifying weak- and strong-segregation block copolymer theories, Macromolecules **29**, 1091 (1996).

[9] E. W. Cochran, C. J. Garcia-Cervera, and G. H. Fredrickson, Stability of the gyroid phase in diblock copolymers at strong segregation, Macromolecules **39**, 2449 (2006).

[10] M. W. Matsen, Equilibrium behavior of asymmetric ABA triblock copolymer melts, J. Chem. Phys. **113**, 5539 (2000).

[11] M. W. Matsen, Effect of architecture on the phase behavior of AB-type block copolymer melts, Macromolecules **45**, 2161 (2012).

[12] A. K. Khandpur, S. Foerster, F. S. Bates, I. W. Hamley, A. J. Ryan, W. Bras, K. Almdal, and K. Mortensen, Polyisoprene-polystyrene diblock copolymer phase diagram near the order-disorder transition, Macromolecules **28**, 8796 (1995).

[13] S.-M. Mai, W. Mingvanish, S. C. Turner, C. Chaibundit, J. P. A. Fairclough, F. Heatley, M. W. Matsen, A. J. Ryan, and C. Booth, Microphase-separation behavior of triblock copolymer melts. Comparison with diblock copolymer melts, Macromolecules **33**, 5124 (2000).

[14] P. Medapuram, J. Glaser, and D. C. Morse, Universal phenomenology of symmetric diblock copolymers near the order-disorder transition, Macromolecules **48**, 819 (2015).

[15] G. H. Fredrickson, Noncircular Wigner-Seitz cells in strongly segregated block copolymers, Macromolecules **26**, 4351 (1993).

[16] S. Lee, M. J. Bluemle, and F. S. Bates, Discovery of a Frank-Kasper σ phase in sphere-forming block copolymer melts, Science **330**, 349 (2010).

[17] K. Kim, M. W. Schulze, A. Arora, R. M. Lewis, M. A. Hillmyer, K. D. Dorfman, and F. S. Bates, Thermal processing of diblock copolymer melts mimics metallurgy, Science **356**, 520 (2017).

[18] S. Lee, C. Leighton, and F. S. Bates, Sphericity and symmetry breaking in the formation of Frank-Kasper phases from one component materials, Proc. Natl. Acad. Sci. USA **111**, 17723 (2014).

[19] A. Reddy, M. S. Dimitriyev, and G. M. Grason, Medial packing and elastic asymmetry stabilize the double-gyroid in block copolymers, Nat. Commun. **13**, 2629 (2022).

[20] M. Rappolt, F. Cacho-Nerin, C. Morello, and A. Yaghmur, How the chain configuration governs the packing of inverted micelles in the cubic $Fd3m$-phase, Soft Matter **9**, 6291 (2013).

[21] K. D. Dorfman, Frank-Kasper phases in block polymers, Macromolecules **54**, 10251 (2021).

[22] A. Reddy, M. B. Buckley, A. Arora, F. S. Bates, K. D. Dorfman, and G. M. Grason, Stable Frank-Kasper phases of self-assembled, soft matter spheres, Proc. Natl. Acad. Sci. USA **115**, 10233 (2018).

[23] S. A. Kim, K.-J. Jeong, A. Yethiraj, and M. K. Mahanthappa, Low-symmetry sphere packings of simple surfactant micelles induced by ionic sphericity, Proc. Natl. Acad. Sci. USA **114**, 4072 (2017).

[24] B. Li, D. Zhou, and Y. Han, Assembly and phase transitions of colloidal crystals, Nat. Rev. Mater. **1**, 15011 (2016).

[25] M. W. Bates, J. Lequieu, S. M. Barbon, R. M. Lewis, K. T. Delaney, A. Anastasaki, C. J. Hawker, G. H. Fredrickson, and C. M. Bates, Stability of the A15 phase in diblock copolymer melts, Proc. Natl. Acad. Sci. USA **116**, 13194 (2019).

[26] T. M. Gillard, S. Lee, and F. S. Bates, Dodecagonal quasicrystalline order in a diblock copolymer melt, Proc. Natl. Acad. Sci. USA **113**, 5167 (2016).

[27] A. J. Mueller, A. P. Lindsay, A. Jayaraman, T. P. Lodge, M. K. Mahanthappa, and F. S. Bates, Quasicrystals and their approximants in a crystalline-amorphous diblock copolymer, Macromolecules **54**, 2647 (2021).

[28] A. B. Chang and F. S. Bates, Impact of architectural asymmetry on Frank-Kasper phase formation in block polymer melts, ACS Nano **14**, 11463 (2020).

[29] M. W. Schulze, R. M. Lewis, J. H. Lettow, R. J. Hickey, T. M. Gillard, M. A. Hillmyer, and F. S. Bates, Conformational asymmetry and quasicrystal approximants in linear diblock copolymers, Phys. Rev. Lett. **118**, 207801 (2017).

[30] G. M. Grason and R. D. Kamien, Interfaces in diblocks: A study of miktoarm star copolymers, Macromolecules **37**, 7371 (2004).

[31] N. Xie, W. Li, F. Qiu, and A.-C. Shi, σ phase formed in conformationally asymmetric AB-type block copolymers, ACS Macro Lett. **3**, 906 (2014).

[32] M. W. Bates, S. M. Barbon, A. E. Levi, R. M. Lewis, III, H. K. Beech, K. M. Vonk, C. Zhang, G. H. Fredrickson, C. J. Hawker, and C. M. Bates, Synthesis and self-assembly of AB_n miktoarm star polymers, ACS Macro Lett. **9**, 396 (2020).

[33] M. Watanabe, Y. Asai, J. Suzuki, A. Takano, and Y. Matsushita, Frank-Kasper A15 phase formed in AB_n block-graft copolymers with large numbers of graft chains, Macromolecules **53**, 10217 (2020).

[34] S. M. Barbon, J.-A. Song, D. Chen, C. Zhang, J. Lequieu, K. T. Delaney, A. Anastasaki, M. Rolland, G. H. Fredrickson, M. W. Bates *et al.*, Architecture effects in complex spherical assemblies of $(AB)_n$-type block copolymers, ACS Macro Letters **9**, 1745 (2020).

[35] M. G. Karavolias, J. B. Elder, E. M. Ness, and M. K. Mahanthappa, Order-to-disorder transitions in lamellar melt self-assembled core-shell bottlebrush polymers, ACS Macro Lett. **8**, 1617 (2019).

[36] See Supplemental Material at http://link.aps.org/supplemental/10.1103/PhysRevMaterials.8.015603 for detailed synthesis protocols and associated ^{1}H NMR and SEC characterization, detailed description of SAXS sample preparation and data acquisition, and estimation of the statistical segment length of poly(ε-decalactone).

[37] K. S. Anderson and M. A. Hillmyer, Melt chain dimensions of polylactide, Macromolecules **37**, 1857 (2004).

[38] M. T. Martello, D. K. Schneiderman, and M. A. Hillmyer, Synthesis and melt processing of sustainable poly(ε-decalactone)-*block*-poly(lactide) multiblock thermoplastic elastomers, ACS Sust. Chem. Eng. **2**, 2519 (2014).

[39] G. L. Baker, E. B. Vogel, and M. R. Smith, Glass transitions in polylactides, Polym. Rev. **48**, 64 (2008).

[40] D. K. Schneiderman, E. M. Hill, M. T. Martello, and M. A. Hillmyer, Poly(lactide)-*block*-poly(ε-caprolactone-*co*-ε-decalactone)-*block*-poly(lactide) copolymer elastomers, Polym. Chem. **6**, 3641 (2015).

[41] A. Yamamoto, Crystallography of quasiperiodic crystals, Acta Cryst. A. **52**, 509 (1996).

[42] T. Ishimasa, S. Iwami, N. Sakaguchi, R. Oota, and M. Mihalkovič, Phason space analysis and structure modelling of 100 Å-scale dodecagonal quasicrystal in Mn-based alloy, Philos. Mag. **95**, 3745 (2015).

[43] F. S. Bates, Measurement of the correlation hole in homogeneous block copolymer melts, Macromolecules **18**, 525 (1985).

[44] S. Lee, T. M. Gillard, and F. S. Bates, Fluctuations, order, and disorder in short diblock copolymers, AIChE J. **59**, 3502 (2013).

[45] R. Vargas, P. Mariani, A. Gulik, and V. Luzzati, Cubic phases of lipid-containing systems: The structure of phase Q^{223} (space group *Pm3n*). An x-ray scattering study, J. Mol. Biol. **225**, 137 (1992).

[46] V. Percec and D. Sahoo, Discotic liquid crystals 45 years later. Dendronized discs and crowns increase liquid crystal complexity to columnar from spheres, cubic Frank-Kasper, liquid quasicrystals and memory-effect induced columnar-bundles, Giant **12**, 100127 (2022).

[47] D. V. Perroni and M. K. Mahanthappa, Inverse $pm\bar{3}n$ cubic micellar lyotropic phases from zwitterionic triazolium gemini surfactants, Soft Matter **9**, 7919 (2013).

[48] K. A. Cavicchi and T. P. Lodge, Self-diffusion and tracer diffusion in sphere-forming block copolymers, Macromolecules **36**, 7158 (2003).

[49] K. A. Cavicchi and T. P. Lodge, Anisotropic self-diffusion in block copolymer cylinders, Macromolecules **37**, 6004 (2004).

[50] K. Kim, A. Arora, R. M. Lewis, M. Liu, W. Li, A.-C. Shi, K. D. Dorfman, and F. S. Bates, Origins of low-symmetry phases in asymmetric diblock copolymer melts, Proc. Natl. Acad. Sci. USA **115**, 847 (2018).

[51] S.-H. Choi, T. P. Lodge, and F. S. Bates, Mechanism of molecular exchange in diblock copolymer micelles: Hypersensitivity to core chain length, Phys. Rev. Lett. **104**, 047802 (2010).

[52] Z. Li and E. E. Dormidontova, Equilibrium chain exchange kinetics in block copolymer micelle solutions by dissipative particle dynamics simulations, Soft Matter **7**, 4179 (2011).

[53] S. J. Dalsin, T. G. Rions-Maehren, M. D. Beam, F. S. Bates, M. A. Hillmyer, and M. W. Matsen, Bottlebrush block polymers: Quantitative theory and experiments, ACS Nano **9**, 12233 (2015).

[54] C. M. Bates, A. B. Chang, N. Momčilović, S. C. Jones, and R. H. Grubbs, ABA triblock brush polymers: Synthesis, self-assembly, conductivity, and rheological properties, Macromolecules **48**, 4967 (2015).

[55] A. L. Liberman-Martin, A. B. Chang, C. K. Chu, R. H. Siddique, B. Lee, and R. H. Grubbs, Processing effects on the self-assembly of brush block polymer photonic crystals, ACS Macro Lett. **10**, 1480 (2021).

[56] F. S. Bates, M. F. Schulz, A. K. Khandpur, S. Förster, J. H. Rosedale, K. Almdal, and K. Mortensen, Fluctuations, conformational asymmetry and block copolymer phase behaviour, Faraday Discuss. **98**, 7 (1994).

[57] F. S. Bates and G. H. Fredrickson, Conformational asymmetry and polymer-polymer thermodynamics, Macromolecules **27**, 1065 (1994).

[58] L. J. Fetters, D. J. Lohse, D. Richter, T. A. Witten, and A. Zirkel, Connection between polymer molecular weight, density, chain dimensions, and melt viscoelastic properties, Macromolecules **27**, 4639 (1994).

[59] T. P. Lodge and P. C. Hiemenz, *Polymer Chemistry*, 3rd ed. (CRC Press, Boca Raton, 2020).

[60] C. Zhang, D. L. Vigil, D. Sun, M. W. Bates, T. Loman, E. A. Murphy, S. M. Barbon, J.-A. Song, B. Yu, G. H. Fredrickson *et al.*, Emergence of hexagonally close-packed spheres in linear block copolymer melts, J. Amer. Chem. Soc. **143**, 14106 (2021).

[61] M. Liu, Y. Qiang, W. Li, F. Qiu, and A.-C. Shi, Stabilizing the Frank-Kasper phases via binary blends of AB diblock copolymers, ACS Macro Lett. **5**, 1167 (2016).

[62] A. P. Lindsay, G. K. Cheong, A. J. Peterson, S. Weigand, K. D. Dorfman, T. P. Lodge, and F. S. Bates, Complex phase behavior in particle-forming AB/AB′ diblock copolymer blends with variable core block lengths, Macromolecules **54**, 7088 (2021).

[63] H. Takagi, R. Hashimoto, N. Igarashi, S. Kishimoto, and K. Yamamoto, Frank-Kasper σ phase in polybutadiene-poly(ε-caprolactone) diblock copolymer/polybutadiene blends, J. Phys.: Condens. Matter **29**, 204002 (2017).

[64] A. J. Mueller, A. P. Lindsay, A. Jayaraman, S. Weigand, T. P. Lodge, M. K. Mahanthappa, and F. S. Bates, Tuning diblock copolymer particle packing symmetry with variable molecular weight core-homopolymers, Macromolecules **55**, 8332 (2022).

[65] R. M. Lewis, A. Arora, H. K. Beech, B. Lee, A. P. Lindsay, T. P. Lodge, K. D. Dorfman, and F. S. Bates, Role of chain length in the formation of Frank-Kasper phases in diblock copolymers, Phys. Rev. Lett. **121**, 208002 (2018).

[66] A. E. Levi, J. Lequieu, J. D. Horne, M. W. Bates, J. M. Ren, K. T. Delaney, G. H. Fredrickson, and C. M. Bates, Miktoarm stars via grafting-through copolymerization: Self-assembly and the star-to-bottlebrush transition, Macromolecules **52**, 1794 (2019).

[67] J. Paturej, S. S. Sheiko, S. Panyukov, and M. Rubinstein, Molecular structure of bottlebrush polymers in melts, Sci. Adv. **2**, e1601478 (2016).

[68] J. M. Chan, A. C. Kordon, R. Zhang, and M. Wang, Direct visualization of bottlebrush polymer conformations in the solid state, Proc. Natl. Acad. Sci. USA **118**, e2109534118 (2021).

[69] E. Panagiotou, K. T. Delaney, and G. H. Fredrickson, Theoretical prediction of an isotropic to nematic phase transition in bottlebrush homopolymer melts, J. Chem. Phys. **151**, 094901 (2019).